Effect of Nanoslit Confinement on the Knotting Probability of Circular DNA

Liang Dai,[†] Johan R. C. van der Maarel,[†,‡] and Patrick S. Doyle*[,†,§]

[†]BioSystems and Micromechanics (BioSyM) IRG, Singapore-MIT Alliance for Research and Technology (SMART) Centre, 3 Science Drive 2, Republic of Singapore 117543

[‡]Department of Physics, National University of Singapore, 2 Science Drive 3, Republic of Singapore 117551

[§]Department of Chemical Engineering, Massachusetts Institute of Technology (MIT), Cambridge, Massachusetts 02139, United States

ⓢ *Supporting Information*

ABSTRACT: Monte Carlo simulations are used to study the knotting probability of circular DNA confined in a slit. We systematically vary the slit height, the width, and the contour length of the DNA molecule. We find that the trend in knotting probability with respect to slit height can be monotonic or nonmonotonic, depending on the width and contour length. The nonmonotonic trend is caused by two competing factors: the increase of the effective persistence length and the increase of segment density by slit confinement. These factors are antagonistic, in the sense that the increase in effective persistence length disfavors knot formation, whereas the increase in segment density favors the knotting probability. Our simulation results bring to light the importance of both chain length and width for slit-confined circular DNA and can be used to guide future experiments which aim to produce populations of knotted DNA through cyclization or catalyzed double-strand passage reactions in confinement.
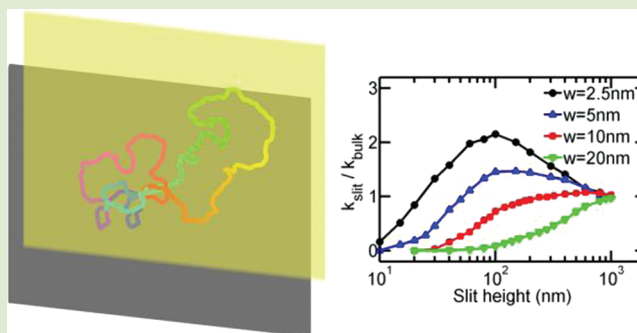
DNA behavior in nanoconfinement is a burgeoning research area. The motivation has been multifold. First, nanodevices with well-defined canonical geometries (e.g., tubes, channels, and slits) provide platforms for fundamental studies of the static and dynamic properties of polymers in confinement.[1−11] Second, the understanding of DNA behavior in nanodevices can be applied to genome analysis.[12−14] Third, in vivo DNA routinely experiences a confined environment due to quasi-stationary membranes and filaments in cells. Confinement in turn can affect the biological function of DNA. For example, DNA confined in a viral capsid experiences a high pressure which can eject the DNA into bacteria during the infection process.[15]

For a linear DNA chain, the effect of confinement on the conformation has extensively been studied using theories,[16−18] simulations,[19−21] and experiments.[1−3] For a circular DNA molecule, the effects of confinement are more complicated, due to the interplay of geometrical confinement and topological constraint (see ref 22 for a review). Such interplay may contribute to the spatial organization of DNA in cells.[23−25] Circular DNA may also be knotted,[26−29] which affects its statics and dynamics. The formation of knots results from either cyclization[30] or double-strand passage reactions catalyzed by type II topoisomerase.[31] The knotting probability, which is defined as the fraction of knotted conformations from all circular conformations, depends on the contour length and the effective diameter of the DNA molecule.[26,30] In vivo, the knotting probability is actively controlled by type II topoisomerases, because the knotting probability was found to be as much as 80 times lower than at thermodynamic equilibrium.[31] The knotting probability was also observed to be dramatically enhanced by confinement inside the capsid of viruses.[32] A virus capsid produces a nearly isotropic, spherical confinement. Computer simulations show that the knotting probability in spherical confinement monotonically increases with increasing confinement.[33]

In contrast to spherical confinement, the knotting probability in slit confinement (a form of uniaxial confinement) can be nonmonotonic with increasing degree of confinement. Recent computer simulations by Micheletti and Orlandini[34] reveal that the knotting probability is initially enhanced several fold by weak and moderate slit confinement and then decreases toward zero in strong slit confinement. In their simulations, the width of the DNA chain is held constant at 2.5 nm and the DNA length varied up to 4.8 μm. This chain width corresponds to DNA at high ionic strength. In experiments or in vivo, the effective chain width may be much larger than 2.5 nm due to decreased screening in the electrostatic double layer.

In our work, we perform Monte Carlo simulations of circular DNA in slits and vary both the chain width and the contour length. The protocol allows double-strand passage (crossing of duplex), which simulates some aspects of type II topoisomerase activity as well as the cyclization of linear chains. The knotting probability calculated from simulations corresponds to the fraction of knotted conformations in circular DNA which are obtained from cyclization experiments.[26,30] We find that the effect of slit confinement on the knotting probability may be nonmonotonic or monotonic, depending on chain width and contour length. We show that this trend arises from a competition between the effective persistence length and segment density in slit confinement.

The simulation method is almost identical to the one we recently used for linear DNA in a slit,[20] except for some modifications for the modeling of circular DNA. Here, we briefly describe the simulation method. DNA is modeled as a ring chain of N beads connected by N inextensible bonds of length l_B, corresponding to a contour length $L = Nl_B$. There are three types of interactions in the simulations: the hard-core repulsion between DNA beads, the hard-core repulsion between DNA beads and slit walls, and the bending energy between adjacent bonds. The hard-core diameter of the bead is set to equal the bond length l_B. The bead diameter is equivalent to the chain width w, such that the number of beads equals L/w. The values w = 5, 10, and 20 nm correspond to ionic strengths of approximately 160, 28, and 6 mM, respectively.[8] The contour length is varied from 2 μm ($\sim$6 kbp) to 16 μm ($\sim$47 kbp). For comparison, P4 phage DNA ($\sim$10 kbp) is often used to study the knotting in experiments[30] and capsids.[27,32] The bending rigidity is set to reproduce a persistence length of 50 nm. We do not consider the twist energy of the circular DNA, so that our model corresponds to a nicked open-circular DNA (similar to what was performed in ref 34).

The simulation starts from an unknotted conformation. We perform one crankshaft move in each Monte Carlo cycle. The crankshaft move may switch an unknotted conformation to a knotted conformation, or the converse. We do not prevent such a move, to obtain the knotting probability, just like the simulations by Micheletti and Orlandini.[34] The DNA conformations sampled by this method correspond to DNA rings obtained by randomly cyclizing linear DNA.[26,30] The simulation usually reaches equilibrium in 10^5 steps. In the production run, we perform 10^{10} steps and record the configuration every 10^5 steps for data analysis. For the estimation of the error in the calculation of knotting probability, we divide the 10^5 configurations into 10 bins, calculate the average knotting probability in each bin, and then calculate the standard deviation of these 10 values (see the Supporting Information). The errors calculated in this way are usually less than the symbol size in the figures, and most of our figures do not show the error bars. We check whether or not the circular DNA is knotted by the Alexander polynomial $\Delta(t)$, following Vologodskii et al.[35] In the current study, we do not classify the knot type.

First, we present the simulation results in bulk. Figure 1 shows the knotting probability k_{bulk} as a function of the contour length. As the chain becomes longer, the knotting probability becomes larger. Similar results have been reported in experiments[26] and computer simulations.[30] In addition, as the chain width w becomes larger, the knotting probability decreases. The dependence of k_{bulk} on w has been used to infer the effective diameter of DNA from the knotting
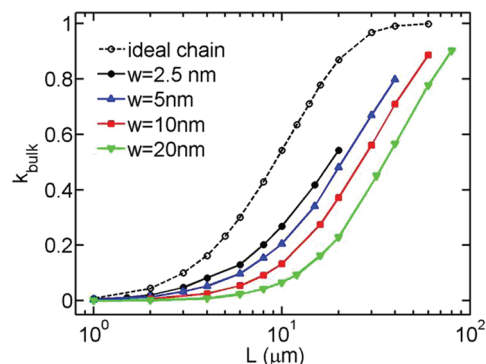

Figure 1. Knotting probability in bulk, k_{bulk}, as a function of the DNA contour length. Different colors (or symbols) correspond to different chain widths. w = 0 corresponds to an ideal chain.

probability in the condition of different ionic strengths.[30] The chain width w = 0 corresponds to an ideal chain in which repulsion between DNA beads is turned off in the simulation.

Next, we proceed to the simulation results of a circular DNA in a slit. Figure 2 shows the knotting probability k_{slit} as a
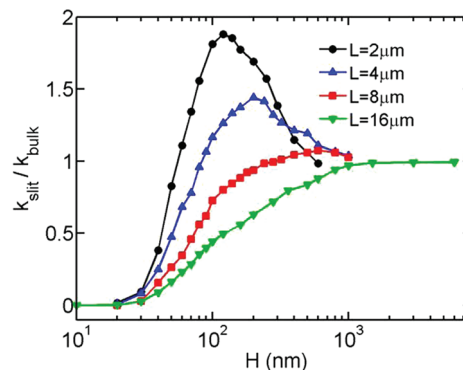

Figure 2. Normalized knotting probability as a function of the slit height. Different colors (or symbols) correspond to different contour length. The chain width is 10 nm for all curves.

function of the slit height. Different curves correspond to simulations using different contour lengths, but with the same chain width w = 10 nm. The knotting probability is normalized to the value in bulk. When the contour length is shorter than about 8 μm, the slit confinement has a nonmonotonic effect on the knotting probability. A similar trend has been observed in the simulations by Micheletti and Orlandini.[34,36] However, when the contour length is 16 μm, increased confinement always reduces the probability for knot formation. As the chain length increases, the peak value of k_{slit}/k_{bulk} becomes smaller, and the peak position shifts to larger slit heights.

We now move on to study the effect of chain width. Figure 3 shows simulation results obtained by using different chain widths, but with a fixed contour length of 8 μm. When the chain width is less than or equal to 10 nm, the knotting probability is nonmonotonic. However, when the chain width is 20 nm, the trend becomes monotonic. As the chain width increases, the peak value of k_{slit}/k_{bulk} becomes smaller, and the peak position shifts to larger slit heights. In the case of an ideal chain (no excluded volume), k_{slit} increases from k_{bulk} in weak and moderate confinement and slightly decreases from the peak value in strong confinement. An ideal chain confined to a plane can cross itself, and thus the knotting probability does not
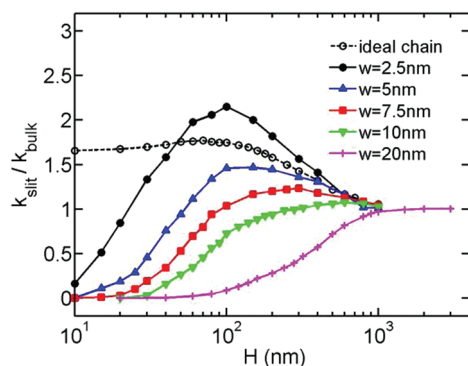
Figure 3. Normalized knotting probability as a function of the slit height. Different colors (or symbols) correspond to different chain widths. The contour length is 8 μm for all curves.

approach zero when H approaches zero, as shown by the dashed line in Figure 3. Note that the ideal chain is not the limiting case for a real chain with a vanishingly small width, because a real chain can never cross itself when confined to a plane, no matter how small the chain width becomes.

The peak positions in Figures 2 and 3 are related to the confinement strength, that is, the ratio of the slit height to the radius of gyration of a chain in bulk. For a thicker or longer chain, the radius of gyration in bulk is larger, and so the peak shifts to a larger slit height. In the Supporting Information, we normalized the slit height to the radius of gyration of DNA in bulk and replot Figures 2 and 3. The peak position in the different curves occurs approximately when H is on the order of the bulk radius of gyration. In addition, we also show the peak value and peak position as a function of the contour length and width in the Supporting Information.

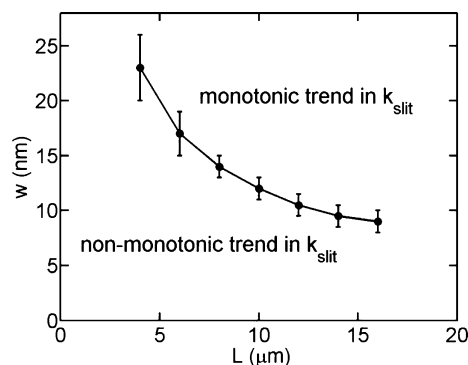Combining the information in Figures 2 and 3, we can create a plot (Figure 4) which generalizes the effect of slit

Figure 4. Diagram of the effect of slit confinement on the knotting probability as a function of the width and the contour length. The curve demarcates the boundary between the monotonic and the nonmonotonic k_{slit} versus H regions.

confinement on the knotting probability as a function of chain width and contour length. The curve demarcates the boundary of the nonmonotonic and monotonic regions. Above the curve, that is, for long and thick chains, the slit confinement monotonically decreases the knotting probability. Below the curve, the knotting probability exhibits a nonmonotonic trend when varying the slit height. Practically, it is difficult to obtain the boundary for a very short or very long chain. For a very short and thick chain (the left-hand end of the curve in Figure

4), the knotting probability is too small (less than 1%) to obtain the precise value. For a very long chain, the computational time becomes impractical. It is expected that for an infinitely long chain the critical chain width approaches zero. This is because the knotting probability of an infinite long chain in bulk is 1,[37] and the knotting probability in a slit cannot exceed this value. With decreasing L, the critical chain width increases more rapidly. However, the critical chain width cannot increase to infinity, because it must be less than the contour length. The nonmonotonic trend will occur for short and thin chains, such as those used in the simulations by Micheletti and Orlandini.[34]

To determine the mechanism for the nonmonotonic trend, we have analyzed some other quantities of the DNA conformation in the simulations. First, we consider the average segment density $\overline{C}_{seg}$ as a function of the slit height. The segment density is inversely proportional to the chain volume. Here, the volume occupied by the chain is defined as the product of the three eigenvalues of the radius of gyration tensor, instead of the radius of gyration cubed R_g^3, because DNA conformations in slits are significantly anisotropic. As shown in Figure 5a, the segment density monotonically
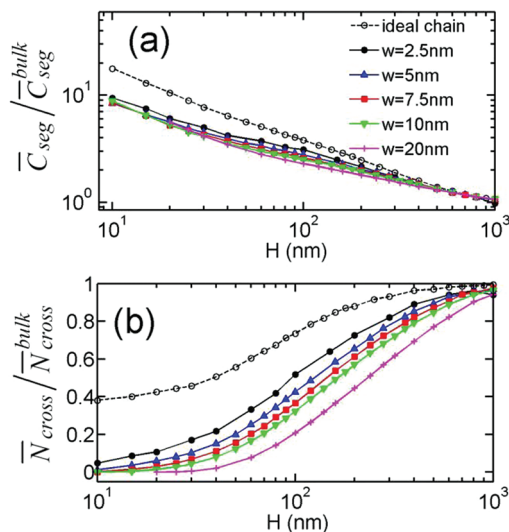

Figure 5. (a) Normalized DNA segment density as a function of the slit height. (b) Number of crossings as a function of the slit height. $\overline{N}_{cross}$ is the average number of crossings for the chain projection on a slit wall, which is normalized to the bulk value. Different symbols (colors) correspond to the simulations using different chain widths and the same contour length of 8 μm.

increases as the slit confinement becomes stronger. The increase in segment density favors knot formation. Note that if we use R_g^3 to infer the segment density, we observe nonmonotonic change of R_g^3 as a function of H, which agrees with the results by Micheletti and Orlandini.[34] However, R_g^3 does not accurately reflect the chain volume.

Next, we calculate the average number of self-crossing events $\overline{N}_{cross}$ when we project the DNA chain on the slit wall, as shown in Figure 5b. Note that $\overline{N}_{cross}$ here is not the number of crossings used for the knot classification, because most of the self-crossings can be removed by three types of Reidemeister moves[38] in knot simplification. $\overline{N}_{cross}$ is normalized to the bulk value $\overline{N}_{cross}^{bulk}$. In bulk, we choose a random direction to project DNA before counting the number of crossings. The values of $\overline{N}_{cross}^{bulk}$ are 77.6, 66.6, 59.0, 63.6, and 39.5, when w = 2.5, 5, 7.5,

10, and 20 nm, respectively. $\bar{N}_{cross}$ monotonically decreases as the slit height decreases. Since $\bar{N}_{cross}$ is positively correlated with the knotting probability, the decrease of $\bar{N}_{cross}$ by slit confinement disfavors knot formation.

The nonmonotonic behavior of the knotting probability in slit confinement appears to be the result of the competing effects of $\bar{N}_{cross}$ and $\bar{C}_{seg}$. However, as shown in Figure 4, the slit confinement monotonically decreases the knotting probability for a sufficiently thick chain or a sufficiently long chain. The monotonic trend is most likely because the disfavoring factor of knotting formation (decrease of $\bar{N}_{cross}$) overwhelms the favoring factor (increase of $\bar{C}_{seg}$) for the whole range of decreasing H (increase in confinement). As shown in Figure 5a,b, for a thicker chain, the favoring factor becomes weaker, and the disfavoring factor becomes stronger. This may be the reason for the monotonic trend when the chain width is sufficiently large. In addition, the competition of the (dis)-favoring factors should also depend on the value of k_{bulk}. For a long chain, k_{bulk} is large, and then the knotting probability is relatively difficult to increase by slit confinement. As mentioned above, the limiting case is that when the chain is infinitely long with a maximal knotting probability of unity. Accordingly, for a sufficiently long chain the knotting probability decreases monotonically with increasing slit confinement.

The increase of $\bar{C}_{seg}$ by slit confinement is relatively easy to understand. The decrease of $\bar{N}_{cross}$ by slit confinement is due to the increase of the effective persistence length by slit confinement. For an ideal chain, our previous simulations show that the effective persistence length monotonically increases when the slit height decreases.[20] The effective persistence length is extracted from the exponential decay of the correlation of segment orientation. For a real chain, the effective persistence length is also observed to be increased greatly by slit confinement in strong confinement regime.[39] In addition, the excluded volume interaction prohibits the self-crossing of a real chain when the slit height is less than the chain width. As a result, for a real chain $\bar{N}_{cross}$ approaches zero when H approaches zero.

Our simulations demonstrate the interplay of spatial confinement and topological states. Slit confinement increases the segment density, which favors knot formation. On the other hand, with decreasing slit height, the effective persistence length of DNA increases from L_p in bulk to $2L_p$ in a plane. This increase in orientation correlation length disfavors knot formation. The excluded volume interaction is also of importance, because it greatly decreases the knotting probability in strong confinement. Overall, the results reveal that all four lengths of the system, that is, persistence length, chain width, contour length, and slit height, play essential roles in determining the knotting probability. The competition of different interactions gives rise to the nonmonotonic or monotonic trend in the knotting probability. Different modes of confinements (e.g., sphere, tube, slit) will in turn have different effects on DNA behavior, because the competitions of different interactions will vary. For instance, previous experimental results reveal that the tube and slit confinements have different effects on DNA compaction induced by depletion.[9,10] Spherical confinement monotonically increases the knotting probability,[33] which is different from the effect of slit confinement. Thus, it would be interesting to examine the effect of tube confinement on the knotting probability. Analysis of the populations of special knot types in confinement is also

an interesting topic, which has been explored by Micheletti and Orlandini[34] but only for a fixed chain width of 2.5 nm.

Note that in our simulation the Monte Carlo moves allow for a DNA segment to pass through another one. As mentioned previously, the knotting probability calculated here thus corresponds to the fraction of nontrivial knots in the DNA rings cyclized from linear chains.[26,30] The situation may also be realized in the presence of type II topoisomerases. However, type II topoisomerases change the distribution of different topological states by a bias in double-strand passage reactions through the dissipation of energy.[31] In other words, in the presence of type II topoisomerases the distribution in topoisomers differs from the one obtained from random passage reactions. Furthermore, in the absence of cutting enzymes, the topology of circular DNA is of course preserved.[11,40] In this case, slit confinement has no effect on the topological state of DNA.

The simulation results presented here can help to predict experimental conditions to produce knotted DNA through cyclization in confinement. The experiment in a slit rather than in bulk should be more efficient to obtain knotted circular DNA, provided the ionic strength is sufficiently high. For example, in the case of λ-DNA with a contour length of 16 μm, the ionic strength should be larger than 30 mM (i.e., the effective diameter[8] of DNA is less than about 9 nm) to increase the knotting probability by slit confinement.

■ ASSOCIATED CONTENT

Ⓢ Supporting Information

Self-correlation of DNA topology in simulations; normalized knotting probability as a function of the normalized slit height; peak value and peak position of the knotting probability. This material is available free of charge via the Internet at http://pubs.acs.org.

■ AUTHOR INFORMATION

Corresponding Author
*E-mail: pdoyle@mit.edu.

■ ACKNOWLEDGMENTS

■ REFERENCES

(1) Reisner, W.; Morton, K. J.; Riehn, R.; Wang, Y. M.; Yu, Z.; Rosen, M.; Sturm, J. C.; Chou, S. Y.; Frey, E.; Austin, R. H. *Phys. Rev. Lett.* **2005**, *94*, 196101.

(2) Bonthuis, D. J.; Meyer, C.; Stein, D.; Dekker, C. *Phys. Rev. Lett.* **2008**, *101*, 108303.

(3) Tang, J.; Levy, S. L.; Trahan, D. W.; Jones, J. J.; Craighead, H. G.; Doyle, P. S. *Macromolecules* **2010**, *43*, 7368−7377.

(4) Zhang, C.; Zhang, F.; van Kan, J. A.; van der Maarel, J. R. C. *J. Chem. Phys.* **2008**, *128*, 225109.

(5) Kim, Y.; Kim, K. S.; Kounovsky, K. L.; Chang, R.; Jung, G. Y.; de Pablo, J. J.; Jo, K.; Schwartz, D. C. *Lab Chip* **2011**, *11*, 1721−1729.

(6) Balducci, A.; Mao, P.; Han, J. Y.; Doyle, P. S. *Macromolecules* **2006**, *39*, 6273−6281.

(7) Hsieh, C. C.; Balducci, A.; Doyle, P. S. *Macromolecules* **2007**, *40*, 5196−5205.

(8) Hsieh, C. C.; Balducci, A.; Doyle, P. S. *Nano Lett.* **2008**, *8*, 1683−1688.

(9) Jones, J. J.; van der Maarel, J. R.; Doyle, P. S. *Nano Lett.* **2011**, *11*, 5047−5053.

(10) Zhang, C.; Shao, P. G.; van Kan, J. A.; van der Maarel, J. R. C. *Proc. Natl. Acad. Sci.* **2009**, *106*, 16651−16656.

(11) Lin, P. K.; Hsieh, C. C.; Chen, Y. L.; Chou, C. F. *Macromolecules* **2012**, *45*, 2920−2927.

(12) Tegenfeldt, J. O.; Prinz, C.; Cao, H.; Chou, S.; Reisner, W. W.; Riehn, R.; Wang, Y. M.; Cox, E. C.; Sturm, J. C.; Silberzan, P.; Austin, R. H. *Proc. Natl. Acad. Sci.* **2004**, *101*, 10979−10983.

(13) Jo, K.; Dhingra, D. M.; Odijk, T.; de Pablo, J. J.; Graham, M. D.; Runnheim, R.; Forrest, D.; Schwartz, D. C. *Proc. Natl. Acad. Sci.* **2007**, *104*, 2673−2678.

(14) Reisner, W.; Larsen, N. B.; Flyvbjerg, H.; Tegenfeldt, J. O.; Kristensen, A. *Proc. Natl. Acad. Sci.* **2009**, *106*, 79−84.

(15) Gelbart, W. M.; Knobler, C. M. *Science* **2009**, *323*, 1682−1683.

(16) de Gennes, P. G., *Scaling concepts in polymer physics*; Cornell University Press: Ithaca, NY, 1979.

(17) Odijk, T. *Macromolecules* **1983**, *16*, 1340−1344.

(18) Odijk, T. *Phys. Rev. E* **2008**, *77*, 060901.

(19) Wang, Y.; Tree, D. R.; Dorfman, K. D. *Macromolecules* **2011**, *44*, 6594−6604.

(20) Dai, L.; Jones, J. J.; van der Maarel, J. R. C.; Doyle, P. S. *Soft Matter* **2012**, *8*, 2972−2982.

(21) Cifra, P. *J. Chem. Phys.* **2009**, *131*, 224903.

(22) Micheletti, C.; Marenduzzo, D.; Orlandini, E. *Phys. Rep. Rev. Sect. Phys. Lett.* **2011**, *504*, 1−73.

(23) Jun, S.; Mulder, B. *Proc. Natl. Acad. Sci.* **2006**, *103*, 12388−12393.

(24) Fritsche, M.; Heermann, D. W. *Soft Matter* **2011**, *7*, 6906.

(25) Jung, Y.; Jeon, C.; Kim, J.; Jeong, H.; Jun, S.; Ha, B. Y. *Soft Matter* **2012**, *8*, 2095.

(26) Shaw, S. Y.; Wang, J. C. *Science* **1993**, *260*, 533−536.

(27) Arsuaga, J.; Vazquez, M.; McGuirk, P.; Trigueros, S.; Sumners, D.; Roca, J. *Proc. Natl. Acad. Sci.* **2005**, *102*, 9165−9169.

(28) Reith, D.; Cifra, P.; Stasiak, A.; Virnau, P. *Nucleic Acids Res.* **2012**, DOI: 10.1093/nar/gks157.

(29) Marenduzzo, D.; Orlandini, E.; Stasiak, A.; Sumners, D.; Tubiana, L.; Micheletti, C. *Proc. Natl. Acad. Sci.* **2009**, *106*, 22269−22274.

(30) Rybenkov, V. V.; Cozzarelli, N. R.; Vologodskii, A. V. *Proc. Natl. Acad. Sci.* **1993**, *90*, 5307−5311.

(31) Rybenkov, V. V.; Ullsperger, C.; Vologodskii, A. V.; Cozzarelli, N. R. *Science* **1997**, *277*, 690−693.

(32) Arsuaga, J.; Vazquez, M.; Trigueros, S.; Sumners, D.; Roca, J. *Proc. Natl. Acad. Sci.* **2002**, *99*, 5373−5377.

(33) Micheletti, C.; Marenduzzo, D.; Orlandini, E.; Sumners, D. W. *Biophys. J.* **2008**, *95*, 3591−3599.

(34) Micheletti, C.; Orlandini, E. *Macromolecules* **2012**, *45*, 2113−2121.

(35) Vologodskii, A. V.; Levene, S. D.; Klenin, K. V.; Frank-Kamenetskii, M.; Cozzarelli, N. R. *J. Mol. Biol.* **1992**, *227*, 1224.

(36) Tesi, M. C.; Vanrensburg, E. J. J.; Orlandini, E.; Whittington, S. G. *J. Phys. A: Math. Gen.* **1994**, *27*, 347−360.

(37) Sumners, D. W.; Whittington, S. G. *J. Phys. A: Math. Gen.* **1988**, *21*, 1689−1694.

(38) Murasugi, K. *Knot Theory and Its Applications*; Birkhäuser: Boston, 1996.

(39) Cifra, P.; Benkova, Z.; Bleha, T. *Faraday Discuss.* **2008**, *139*, 377−392.

(40) Strychalski, E. A.; Geist, J.; Gaitan, M.; Locascio, L. E.; Stavis, S. M. *Macromolecules* **2012**, *45*, 1602−1611.